30. Hare JM, Stamler JS. NO/redox disequilibrium in the failing heart and cardiovascular system. *J Clin Invest* 2005;**115**:509–517.
31. Dedkova EN, Ji X, Wang YG, Blatter LA, Lipsius SL. Signaling mechanisms that mediate nitric oxide production induced by acetylcholine exposure and withdrawal in cat atrial myocytes. *Circ Res* 2003;**93**:1233–1240.
32. Wink DA, Miranda KM, Espey MG, Pluta RM, Hewett SJ, Colton C *et al.* Mechanisms of the antioxidant effects of nitric oxide. *Antioxid Redox Signal* 2001;**3**:203–213.
33. Mohan RM, Heaton DA, Danson EJ, Krishnan SP, Cai S, Channon KM *et al.* Neuronal nitric oxide synthase gene transfer promotes cardiac vagal gain of function. *Circ Res* 2002;**91**:1089–1091.
34. Li JM, Gall NP, Grieve DJ, Chen M, Shah AM. Activation of NADPH oxidase during progression of cardiac hypertrophy to failure. *Hypertension* 2002; 40:477–484.
35. Nediani C, Borchi E, Giordano C, Baruzzo S, Ponziani V, Sebastiani M *et al.* NADPH oxidase-dependent redox signaling in human heart failure: relationship between the left and right ventricle. *J Mol Cell Cardiol* 2007;**42**:826–834.
36. Shinyashiki M, Pan CJ, Lopez BE, Fukuto JM. Inhibition of the yeast metal reductase heme protein fre1 by nitric oxide (NO): a model for inhibition of NADPH oxidase by NO. *Free Radic Biol Med* 2004;**37**: 713–723.
37. Matsuura W, Sugimachi M, Kawada T, Sato T, Shishido T, Miyano H *et al.* Vagal stimulation decreases left ventricular contractility mainly through negative chronotropic effect. *Am J Physiol* 1997;**273**: H534–H539.
38. Mark AL. Sensitization of cardiac vagal afferent reflexes at the sensory receptor level: an overview. *Fed Proc* 1987;**46**:36–40.

ELSEVIER

Atherosclerosis 196 (2008) 172–179

ATHEROSCLEROSIS

www.elsevier.com/locate/atherosclerosis

Azelnidipine has anti-atherosclerotic effects independent of its blood pressure-lowering actions in monkeys and mice

Kaku Nakano [a], Kensuke Egashira [a,*], Kisho Ohtani [a], Zhao Gang [b], Eiko Iwata [a], Miho Miyagawa [a], Kenji Sunagawa [a]

[a] *Department of Cardiovascular Medicine, Graduate School of Medical Sciences, Kyushu University, Fukuoka, Japan*
[b] *Department of Cardiovascular Medicine, Shanghai Sixth People's Hospital, Shanghai Jiao Tong University Affiliated Sixth People's Hospital, Shanghai, China*

Received 17 October 2006; received in revised form 19 March 2007; accepted 22 March 2007
Available online 3 May 2007

Abstract

Calcium channel blockers (CCBs) have been shown to improve clinical outcomes in atherosclerotic vascular disease. The mechanisms underlying the vasculoprotective effects of a third-generation calcium channel blocker, azelnidipine, are incompletely understood. We asked whether azelnidipine attenuates atherosclerosis in monkeys and mice beyond its blood pressure-lowering effects. Cynomolgus monkeys were randomized to three groups after 4 weeks of a high cholesterol diet: control group (no treatment) and 3 and 10 mg/kg daily azelnidipine; these doses have no effect on systemic arterial pressure or heart rate. Atherosclerosis was induced in the aorta by balloon injury, and the diet and treatment were continued for an additional 24 weeks. Azelnidipine did not affect blood lipid profiles, but reduced the development of atherosclerosis as detected by the elimination of local oxidative stress and reduced expression of monocyte chemoattractant protein-1 and platelet-derived growth factor. Azelnidipine also reduced the proliferation and migration of vascular smooth muscle cells in vitro. In atherosclerotic ApoE-knockout (ApoE-KO) mice fed a high cholesterol diet, azelnidipine but not amlodipine reduced the development of atherosclerosis. Neither drug changed the lipid profiles or systolic blood pressure of the mice. Thus, azelnidipine at clinically relevant doses exhibited anti-atherosclerotic effects in monkeys and mice independent of its blood pressure-lowering effects, suggesting that azelnidipine might be as a "vasculoprotective calcium channel blocker".

Keywords: Atherosclerosis; Calcium channel blockers; Cytokines; Smooth muscle cells; Azelnidipine

1. Introduction

Calcium channel blockers (CCBs) have been used worldwide to treat patients with hypertension and angina pectoris. Recent clinical trials with CCBs, such as PREVENT, ALLHAT, VALUE, CAPARES, ACTION, and CAMELOT, have provided evidence that reducing arterial blood pressure to close to normal ranges is of great importance for reducing cardiovascular events [1–6]. These clinical trials suggest that CCBs may have pleiotropic actions beyond simply lowering blood pressure. The pleiotropic actions of CCBs may be distinct from its pharmacologic actions related to blocking L-type calcium channels, but may be attributable to their lipophilic character, which gives them a high affinity for the membrane phospholipids of arterial wall cells, such as vascular smooth muscle cells (see review by Mason et al. [7]). CCBs' vasculoprotective actions include improvement of endothelial function, anti-inflammation effects, anti-oxidant effects, and anti-proliferation effects on vascular smooth muscle cells (VSMCs).

* Corresponding author at: Department of Cardiovascular Medicine, Graduate School of Medical Sciences, Kyushu University, 3-1-1 Maidashi, Higashi-ku, Fukuoka 812-8582, Japan. Tel.: +81 92 642 5358; fax: +81 92 642 5375.
E-mail address: egashira@cardiol.med.kyushu-u.ac.jp (K. Egashira).

0021-9150/$ – see front matter © 2007 Elsevier Ireland Ltd. All rights reserved.
doi:10.1016/j.atherosclerosis.2007.03.036

In animals, CCBs have been shown to prevent or attenuate atherosclerosis [8], hypertension-induced vascular remodeling, neointimal formation after vascular injury [9]. Azelnidipine is a newly developed third-generation CCB that has anti-hypertensive effects comparable to amlodipine [10]. Azelnidipine is strongly lipophilic and has a high affinity for membrane of vascular wall cells, such as vascular smooth muscle cells [11]. We recently reported that azelnidipine attenuated stent-associated neointimal formation associated with reduced expression of monocyte chemoattractant protein-1 (MCP-1) in non-human primates (cynomolgus monkeys) [12]. In that study, we found that azelnidipine's attenuation of neointimal formation was independent of its blood pressure-lowering actions in vivo, and that azelnidipine directly reduced MCP-1-induced proliferation of VSMC, suggesting that azelnidipine's beneficial effects on in-stent restenosis were mediated in part by direct inhibition of VSMC proliferation. However, the mechanisms of the anti-atherosclerotic action and the clinical significance of azelnidipine were not fully addressed.

The aim of this study is to investigate whether azelnidipine at clinically relevant doses attenuates atherosclerosis in non-human primates (cynomolgus monkeys) in ways that are independent of its blood pressure-lowering effects. To confirm the clinical significance of the findings, we used a non-human primate model of atherosclerosis [13]. Although it is difficult to choose an appropriate animal model for studying atherosclerosis, a non-human primate model may have an advantage over non-primate animal models, such as rabbits and mice: vascular inflammatory and proliferative responses to injury in non-human primates are presumed to be more similar to those in humans than are those of other non-primate animals. Therefore, the use of non-human primates may allow us to evaluate the efficacy of any therapies on atherosclerosis in clinically relevant conditions. Furthermore, to examine whether the observed anti-atherosclerotic effects are unique to azelnidipine or are a class-effect of CCBs, we also compared the effects of azelnidipine and amlodipine in ApoE-knockout (ApoE-KO) mice.

2. Methods

An enhanced Methods and Results section is available online at doi:10.1016/J.atherosclerosis.2007.03.036.

2.1. Cynomolgus monkeys: animals and study protocol

The study protocol was reviewed and approved by the Committee on the Ethics of Animal Experiments, Kyushu University Graduate School of Medical Sciences. Thirty-six 5-year-old male cynomolgus monkeys weighing 4.0 – 6.0 kg were purchased from Primate Ltd. (Gaoyao, Guang Dong, China). The monkeys were fed a high cholesterol diet (0.5% cholesterol and 6% corn oil) for 4 weeks prior to the balloon injury operation. Ticlopidine (100 mg) and aspirin (81 mg) were administered each day starting 7 days before the balloon procedure; ticlopidine was administered for 28 days, and aspirin was continued until euthanization at 6 months. The animals were randomized to 3 groups ($n = 12$ monkeys per group) as follows: (1) no treatment/vehicle control group (0.5% carboxymethyl cellulose sodium salt); (2) low-dose azelnidipine group (3 mg/kg per day; donated by Sankyo Pharmaceutical Co., Tokyo, Japan); and (3) high-dose azelnidipine group (10 mg/kg per day). These doses of azelnidipine were selected because we previously reported that first, the 3 and 10 mg/kg doses do not affect systemic arterial pressure and heart rate in conscious monkeys by telemetric measurements; and second, the low dose of azelnidipine used in the present study for monkeys was within clinical range, because the maximum drug concentration (C_{max}) of azelnidipine at 3 and 10 mg/kg per day was 36 ± 17 and 107 ± 17 ng/mL, respectively, in monkeys [12], while the C_{max} after oral administration of azelnidipine at 16 mg in hypertensive human subjects is reported to be 48 ± 19 ng/mL. Azelnidipine was administered to the monkeys once a day by gavage for 24 weeks. One week after starting azelnidipine treatment in the azelnidipine groups, all monkeys were anesthetized with ketamine hydrochloride (10 mg/kg IM) and sodium pentobarbital (30 mg/kg IV). The left femoral artery was surgically exposed, a 4 Fr sheath catheter was passed into the femoral artery, and monkeys received a balloon injury of the thoracic and abdominal aorta, as previously described [13]. The right femoral artery was then ligated and the incision was closed. After the operation, all monkeys were fed the same high cholesterol diet. Animal care before and after the operation took place in Gaoyao Kangda Laboratory Animal Science and Technology in China.

2.2. Comparison of azelnidipine and amlodipine in ApoE-KO mice

Male ApoE-KO mice were purchased from Jackson Laboratory (Bar Harbor, Maine, USA). ApoE-KO mice were fed a Western-type diet (Oriental Yeast, Tokyo, Japan) during the experiment. At 8 weeks of age, mice were randomly assigned into the following groups: (1) no treatment/vehicle control group ($n = 10$); (2) low-dose azelnidipine group (3 mg/kg per day; $n = 6$); (3) high-dose azelnidipine group (10 mg/kg per day; $n = 7$); and (4) amlodipine group (same class CCB; 10 mg/kg per day, donated by Pfizer Japan Inc., Tokyo, Japan; $n = 6$). Azelnidipine and amlodipine treatment was carried out for 8 weeks by mixing the drug with food for the mice. After 8 weeks of treatment, all mice were sacrificed and tissue was prepared for analysis. Tissue preparation was performed as previously described [14]. Briefly, after the mouse was killed, the aorta was rapidly removed from the left ventricle after perfusion with phosphate-buffered saline. The aorta from the arch to the bifurcation of the iliac artery was fixed in 10% buffered formalin for measurement of the surface area covered by lipid-staining lesions. To quantify the extent of the atherosclerotic lesions, adventitial tissue was removed from

the aortic arch and the aortic arch was opened longitudinally, stained with oil red O, and pinned out on a black wax surface. The percentage of the endothelial surface area stained by oil red O was determined [14].

Plasma total cholesterol, high-density lipoprotein cholesterol and triglycerides concentrations were determined using commercially available kits (Wako Pure Chemicals, Tokyo, Japan). Systolic blood pressure and heart rate were measured every other week (by the tail-cuff method [14]). Moreover, to evaluate the safety of azelnidipine, a multiplex immunoassay was performed using the Luminex Lab MAP instrument by Charles River Inc. (see online Supplementary data).

3. Results

3.1. Histopathological and immunohistochemical measurements in monkeys

In the thoracic aorta, treatment with low and high doses of azelnidipine significantly reduced the neointimal area (Fig. 1A and B; vehicle group: $1.86 \pm 0.23\,mm^2$, low-dose group: $0.96 \pm 0.16\,mm^2$, high-dose group: $1.02 \pm 0.19\,mm^2$). These doses also significantly reduced the intima-media ratio (Fig. 1B: vehicle group: 0.45 ± 0.26, low-dose group: 0.23 ± 0.04, high-dose group: $0.28 \pm$

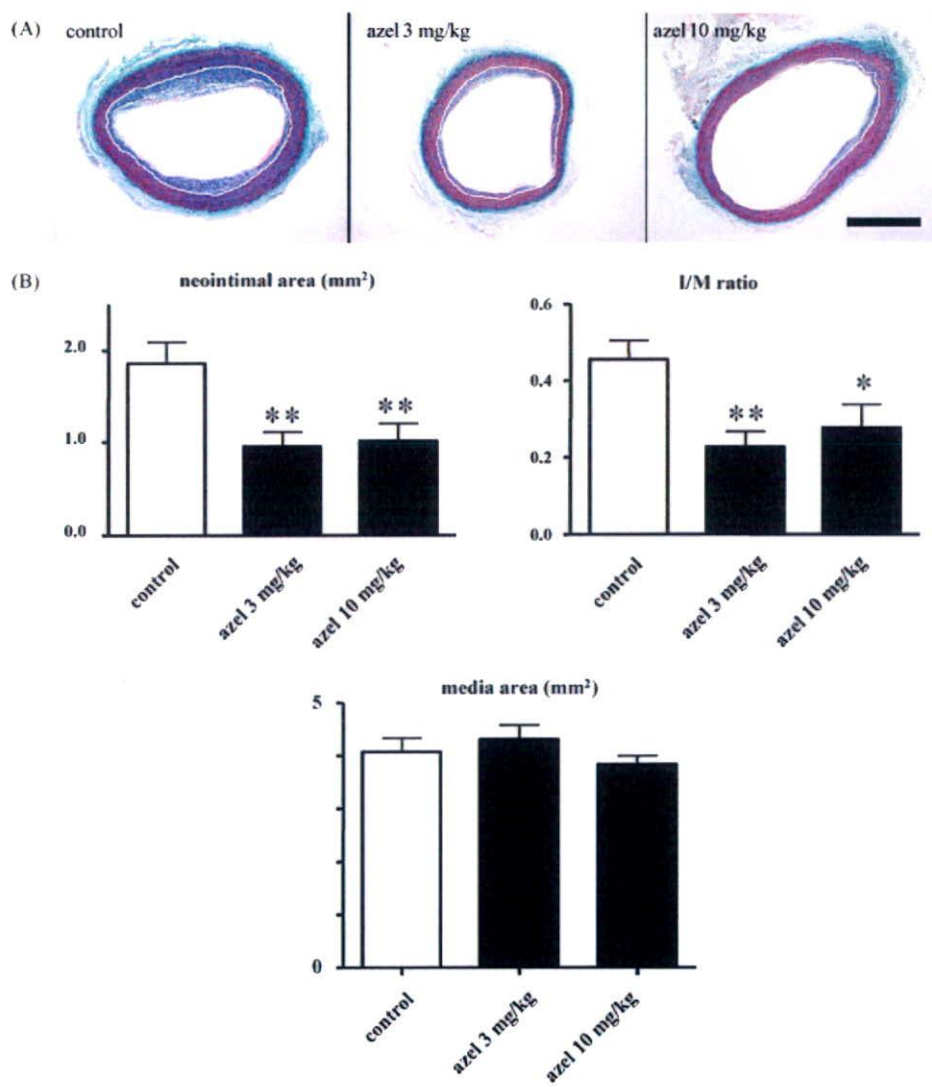

Fig. 1. Effects of azelnidipine on atherosclerosis in monkey thoracic aorta. (A) Representative photomicrographs are shown of Masson's trichrome-stained cross-sections of the injured thoracic aortas from the vehicle control group (control, left panel), low-dose azelnidipine group (azel 3 mg/kg, middle panel) and high-dose azelnidipine group (azel 10 mg/kg, right panel). Internal elastica lamina are outlined with white. Bar = 10 mm. (B) Measurements of the neointimal areas, intima/media (I/M) ratios, and media areas of the thoracic aortas from monkeys treated with or without azelnidipine as indicated ($n = 12$ each). $^*P < 0.05$, $^{**}P < 0.01$ versus vehicle control group. Each value represents mean ± S.E.M.

0.06). There was no difference in media area among the groups.

Immunohistochemical expression of MCP-1 and PDGF-BB and the composition of the neointima were then examined in the abdominal aorta in the neointima (Fig. 2A). Azelnidipine at low and high doses reduced PDGF-BB and MCP-1 expression in the neointima (Fig. 2). In contrast, neither dose of azelnidipine affected the neointimal area (vehicle group:

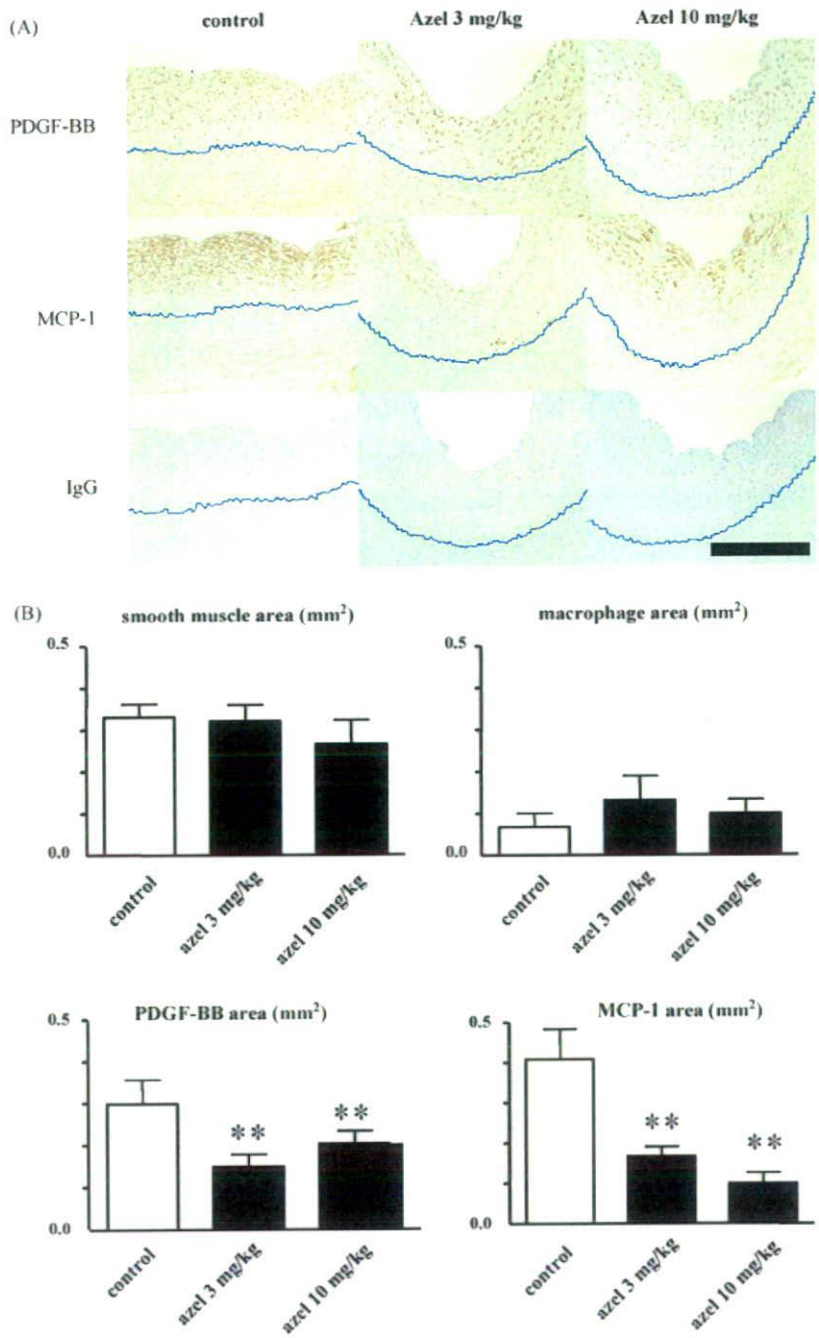

Fig. 2. Immunohistochemical detection of PDGF-BB and MCP-1 expression. (A) Cross-sections of abdominal aortas from experimental groups stained with the antibody against monocyte chemoattractant protein-1 (MCP-1), platelet-derived growth factor (PDGF), or non-immune IgG (negative control). Internal elastica lamina are outlined with blue. Bar = 100 μm. (B) The MCP-1- and PDGF-positive areas were markedly decreased in azelnidipine low- and high-dose groups. However, there were no significant differences in the smooth muscle cell areas and macrophage areas among the groups. $^{**}P < 0.01$ versus vehicle control group ($n = 12$ each). Each value represents mean ± S.E.M.

$1.49 \pm 0.10\,mm^2$, low-dose group: $1.54 \pm 0.15\,mm^2$, high-dose group, $1.27 \pm 0.17\,mm^2$) or the macrophage or smooth muscle areas (Fig. 2B).

3.2. Detection of local oxidative stress in the aorta using DHE staining

No DHE fluorescence was detected in the normal abdominal aorta (data not shown). As shown in Online Figure, the fluorescent signal attributable to superoxide production was markedly enhanced in the neointima and media from the control group. Azelnidipine at low and high doses eliminated the intensity of DHE fluorescence in the neointima (Online Figure), whereas the DHE signal intensity did not differ among three groups in the media (data not shown).

3.3. Proliferation and migration of vascular smooth muscle cells in vitro

Azelnidipine at 1, 10, and 100 nM significantly inhibited the PDGF-induced proliferation of the human coronary smooth muscle cells (Fig. 3A). To examine the effects of azelnidipine on the PDGF-induced release of MCP-1, MCP-1 concentrations in supernatant fluid were measured (Fig. 3B). PDGF increased the MCP-1 levels in supernatant from 462 ± 23 to 1322 ± 98 pg/mL. Azelnidipine at 1, 10, and 100 nM significantly reduced the MCP-1 levels to 548 ± 34, 742 ± 39, and 405 ± 33 pg/mL, respectively (Fig. 3B). Azelnidipine at 1, 10, and 100 nM also inhibited the PDGF-induced migration of rat aortic smooth muscle cells (Fig. 3C). The human coronary arterial smooth muscle cells treated with azelnidipine at 100 nM showed no signs of cell toxicity or apoptosis (data not shown).

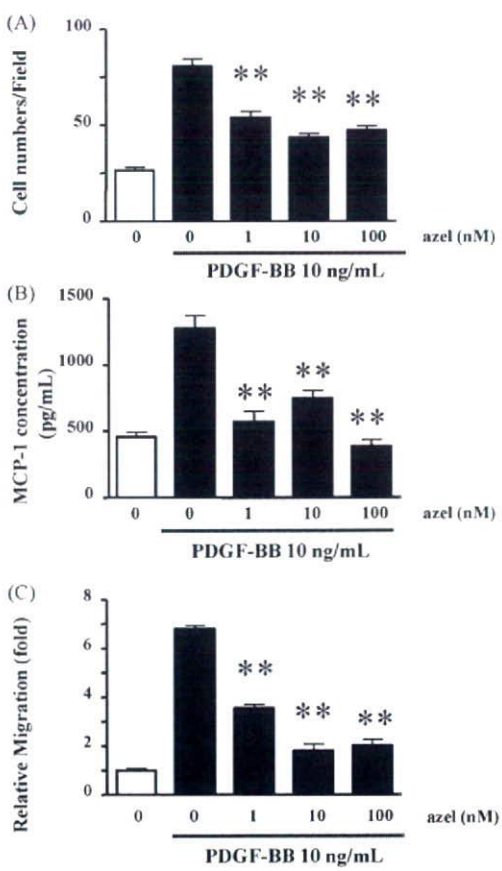

Fig. 3. Effects of azelnidipine on PDGF-induced proliferation of human coronary artery smooth muscle cells (A), on the concentration of MCP-1 in supernatant fluid from cell cultures treated with PDGF-BB (B), and on the migration of rat aortic smooth muscle cells (C). $^*P < 0.01$ versus control ($n = 9$). Each value represents mean ± S.E.M.

3.4. Comparison of azelnidipine and amlodipine in ApoE-KO mice

Azelnidipine at low and high doses markedly reduced atherosclerotic lesion formation as detected by staining of en face preparations of the aortas of ApoE-KO mice (Fig. 4).

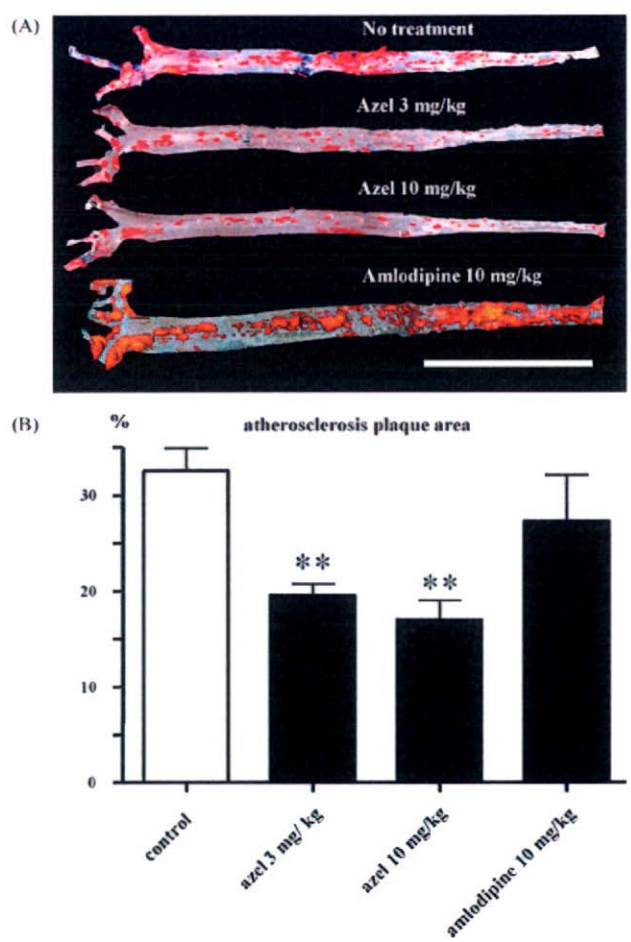

Fig. 4. Effects of azelnidipine and amlodipine on atherosclerosis in ApoE-KO mice. (A) En face preparations of aortas were stained with oil red O. Bar = 10 mm. (B) Quantitative comparison of atherosclerotic lesion size (percent of oil red O stained area) ($n = 6$–10). Data are reported as mean ± S.E.M. $^{**}P < 0.01$ versus no treatment group.

However, amlodipine showed no such reduction compared with the 'no treatment' group (Fig. 4). In contrast, there were no significant differences in the lipid profiles, systolic blood pressure, and heart rates among the differently treated groups of mice (Online Table 2). There were also no significant differences in levels of multiple cytokines and chemokines among the groups (Online Table 3).

4. Discussion

The present study demonstrated that treatment with a newly developed CCB, azelnidipine, at 3 and 10 mg/kg attenuated the development of advanced atherosclerosis induced by balloon injury and hypercholesterolemia in non-human primates (cynomolgus monkeys).

To assess the clinical significance of our present finding, the dose range of azelnidipine is important. We recently reported that the C_{max} of azelnidipine at 3 and 10 mg/kg per day were 36 ± 17 and 107 ± 17 ng/mL, respectively, in cynomolgous monkeys [12]. The C_{max} after oral administration of 16 mg of azelnidipine to hypertensive subjects is reported to be 48 ± 19 ng/mL [10]. Therefore, it is reasonable to consider that in regards to plasma concentrations (C_{max}), the 3 mg/kg dose is within a clinically relevant dose range, and the 10 mg/kg dose is higher than the clinical dose range (i.e. is a pharmacological dose range) in monkeys. Furthermore, we also reported that the dose of azelnidipine used in the present study did not affect systemic arterial blood pressure and heart rate in cynomolgus monkeys under conscious conditions [12]. Therefore, it is suggested that the beneficial effects of azelnidipine on atherosclerosis as observed in monkeys were not due to its effects on serum lipids or arterial blood pressure (Table 1).

To examine the mechanisms underlying azelnidipine's anti-atherosclerotic effects, we examined a representative local oxidative stress marker with fluorescent dihydroethidium staining in monkeys. Our data clearly showed that azelnidipine at low and high doses nearly eliminated the increase in the fluorescence (i.e. the increase in oxidative stress) in neointima cells in atherosclerotic lesions. Similar potent anti-oxidant effects of azelnidipine were also reported by Jinno et al. [9], who showed that azelnidipine prevented the increases in fluorescent dihydroethidium signals and NAD(P)H oxidase activity in the neointima induced by cuff-induced vascular injury. Because the neointima usually consists of activated smooth muscle cells, the present data suggest that mediation of local oxidative stress in neointimal smooth muscle cells is one of the major pathways by which azelnidipine exerts its anti-atherosclerotic actions.

Table 1
Serum MCP-1 levels in cynomolgus monkeys

	Baseline (week 0)	24 weeks after treatment
Control	44 ± 5	61 ± 5*
Azelnidipine 3 mg/kg	46 ± 4	47 ± 5
Azelnidipine 10 mg/kg	47 ± 4	37 ± 4

Data are expressed as mean ± S.E.M. $n = 12$.
* $P < 0.05$ vs. baseline.

Because inflammatory and proliferative processes induced by oxidative stress play a central role in atherogenesis [15], we next used immunohistochemistry to examine the expression of MCP-1 and PDGF. We and others have demonstrated that increased monocyte-mediated inflammation is associated with greater neointimal formation after stenting [16,17] and that anti-MCP-1 gene therapy [18,19] or administration of blocking antibody against the MCP-1 receptor markedly reduces neointimal formation after vascular injury. In addition to inflammation, the proliferation of vascular smooth muscle cells induced by PDGF plays a crucial role in atherogenesis. Here, we found reduced MCP-1 and PDGF immunoreactivity in the neointimal smooth muscle cells after treatment with azelnidipine at 3 and 10 mg/kg. Normalization of serum MCP-1 levels was also noted with azelnidipine treatment. These data suggest that the anti-atherosclerotic effects of azelnidipine might be attributable to the inhibition of oxidative stress-induced upregulation of MCP-1 and PDGF in the neointimal cells.

However, immunohistochemical analysis of the cellular composition of the neointima showed that azelnidipine had no effect on macrophage infiltration. We therefore hypothesized that azelnidipine was having a direct effect on vascular smooth muscle cells. The date presented here from vascular smooth muscle cells in culture shows that azelnidipine significantly inhibits PDFG-induced proliferation and migration of vascular smooth muscle cells. In addition, this inhibitory effect was associated with decreased PDGF-induced production of MCP-1. We recently found that blocking MCP-1 partly inhibits PDGF-induced proliferation and migration of vascular smooth muscle cells in culture (author's unpublished data, 2006). In addition, it was recently reported that MCP-1 not only mediates monocyte-related inflammation, but also mediates transformation, proliferation, and migration of vascular smooth muscle cells [20]. Collectively, these data suggest that MCP-1 is involved in the mechanism of azelnidipine's inhibitory effects on PDGF-induced proliferation and migration of vascular smooth muscle cells.

To investigate whether the observed anti-atherosclerotic effects are unique to azelnidipine, we therefore compared effects of azelinidipine versus amlodipine in ApoE-KO mice. Azelnidipine at 10 mg/kg per day, but not amlodipine at 10 mg/kg per day, reduced atherosclerotic plaque size after 8 weeks of a high cholesterol diet. Neither azelnidipine nor amlodipine had any effect on hemodynamic parameters or on blood lipid profiles, indicating that the observed differential effects between the two drugs are independent of any effects on serum lipid levels or arterial blood pressure. Our present data are not contradictory to previous articles showing no definitive effects in atherosclerositic mice [21,22] or monkeys [23]. The mechanism underlying the differential

effects of these two CCBs is unclear, but may be related to azelnidipine's high lipid solubility/high vascular affinity [23]. Recently, Ma et al. reported that the inhibitory effect of azelnidipine on iNOS-catalyzed NO production from vascular smooth muscle cells in culture was greater than that of amlodipine or nifedipine [24]. Moreover, azelnidipine is reported to inhibit H_2O_2-induced production of 8-iso-prostane from human arterial endothelial cells in culture to a greater extent than other same class CCBs (amlodipine and nifedipine) [25].

There are several caveats in interpreting the clinical significance of our present study. First, although we have shown anti-atherosclerotic effects of azelnidipine in non-human primates, the experimental and clinical evidence for the anti-atherosclerotic effects of CCBs remains controversial. Recent clinical trials with CCBs did not directly address the reduction of atherosclerosis and/or cardiovascular mortality in patients with atherosclerotic vascular disease [26]. Second, it deserves mentioning that the vast majority of patients with atherosclerotic vascular disease is not treated with CCB alone, but with combination of CCB plus statin, angiotensin receptor blockers and etc. [27]. In this regard, recent reports shows a synergistic effects of CCBs and statin etc. on progression of atherosclerosis. It is likely therefore that clinical benefits of CCBs on atherosclerosis might be overt in combination of other vasculoprotective drugs, such as statins.

In conclusion, this study presents experimental evidence that oral administration of azelnidipine at a clinically relevant dose and at a pharmacological dose attenuates advanced atherosclerosis in non-human primates. The beneficial effects were associated with reduced local oxidative stress, reduced MCP-1 and PDGF expression, and reduced smooth muscle cell proliferation/migration in the neointima. Notably, the anti-atherosclerotic effect seems to be unique to azelnidipine, rather than a class-effect of CCBs in respect to our data with ApoE-KO mice. These data in non-human primates suggest potential clinical benefits of azelnidipine might be beneficial as a "vasculoprotective CCB" in patients with atherosclerotic vascular disease. Further clinical trials are needed to prove this hypothesis.

Acknowledgements

This study was supported by Grants-in-Aid for Scientific Research (14657172, 14207036) from the Ministry of Education, Science, and Culture, Tokyo, Japan and by unlimited research grant from Sankyo Co., Tokyo, Japan.

Appendix A. Supplementary data

Supplementary data associated with this article can be found, in the online version, at doi:10.1016/j.atherosclerosis.2007.03.036.

References

[1] Pitt B, Byington RP, Furberg CD, et al. Effect of amlodipine on the progression of atherosclerosis and the occurrence of clinical events. PREVENT Invest Circ 2000;102:1503–10.
[2] Major outcomes in high-risk hypertensive patients randomized to angiotensin-converting enzyme inhibitor or calcium channel blocker vs. diuretic: the Antihypertensive and Lipid-Lowering Treatment to Prevent Heart Attack Trial (ALLHAT). JAMA 2002;288:2981–97.
[3] Julius S, Kjeldsen SE, Weber M, et al. Outcomes in hypertensive patients at high cardiovascular risk treated with regimens based on valsartan or amlodipine: the VALUE randomised trial. Lancet 2004;363:2022–31.
[4] Jorgensen B, Simonsen S, Endresen K, et al. Restenosis and clinical outcome in patients treated with amlodipine after angioplasty: results from the Coronary AngioPlasty Amlodipine REStenosis Study (CAPARES). J Am Coll Cardiol 2000;35:592–9.
[5] Nissen SE, Tuzcu EM, Libby P, et al. Effect of antihypertensive agents on cardiovascular events in patients with coronary disease and normal blood pressure: the CAMELOT study: a randomized controlled trial. JAMA 2004;292:2217–25.
[6] Poole-Wilson PA, Lubsen J, Kirwan BA, et al. Effect of long-acting nifedipine on mortality and cardiovascular morbidity in patients with stable angina requiring treatment (ACTION trial): randomised controlled trial. Lancet 2004;364:849–57.
[7] Mason RP, Marche P, Hintze TH. Novel vascular biology of third-generation L-type calcium channel antagonists: ancillary actions of amlodipine. Arterioscler Thromb Vasc Biol 2003;23:2155–63.
[8] Henry PD, Bentley KI. Suppression of atherogenesis in cholesterol-fed rabbit treated with nifedipine. J Clin Invest 1981;68:1366–9.
[9] Jinno T, Iwai M, Li Z, et al. Calcium channel blocker azelnidipine enhances vascular protective effects of AT1 receptor blocker olmesartan. Hypertension 2004;43:263–9.
[10] Kuramoto K, Ichikawa S, Hirai A, et al. Azelnidipine and amlodipine: a comparison of their pharmacokinetics and effects on ambulatory blood pressure. Hypertens Res 2003;26:201–8.
[11] Yagil Y, Lusting A, Azelnidipine. (CS-905), a novel dihydropyridine calcium channel blocker with gradual onset and prolonged duration of action. Cardiovasc Drugs Rev 1995;13:137–48.
[12] Nakano K, Egashira K, Tada H, et al. A third-generation, long-acting, dihydropyridine calcium antagonist, azelnidipine, attenuates stent-associated neointimal formation in non-human primates. J Hypertens 2006;24:1881–9.
[13] Kitamoto S, Nakano K, Hirouchi Y, et al. Cholesterol-lowering independent regression and stabilization of atherosclerotic lesions by pravastatin and by antimonocyte chemoattractant protein-1 therapy in nonhuman primates. Arterioscler Thromb Vasc Biol 2004;24:1522–8.
[14] Inoue S, Egashira K, Ni W, et al. Anti-monocyte chemoattractant protein-1 gene therapy limits progression and destabilization of established atherosclerosis in apolipoprotein E-knockout mice. Circulation 2002;106:2700–6.
[15] Egashira K. Clinical importance of endothelial function in arteriosclerosis and ischemic heart disease. Circ J 2002;66:529–33.
[16] Farb A, Weber DK, Kolodgie FD, Burke AP, Virmani R. Morphological predictors of restenosis after coronary stenting in humans. Circulation 2002;105:2974–80.
[17] Welt FG, Rogers C. Inflammation and restenosis in the stent era. Arterioscler Thromb Vasc Biol 2002;22:1769–76.
[18] Egashira K, Zhao Q, Kataoka C, et al. Importance of monocyte chemoattractant protein-1 pathway in neointimal hyperplasia after periarterial injury in mice and monkeys. Circ Res 2002;90:1167–72.
[19] Egashira K. Molecular mechanisms mediating inflammation in vascular disease: special reference to monocyte chemoattractant protein-1. Hypertension 2003;41:834–41.
[20] Denger S, Jahn L, Wende P, et al. Expression of monocyte chemoattractant protein-1 cDNA in vascular smooth muscle cells: induction

of the synthetic phenotype: a possible clue to SMC differentiation in the process of atherogenesis. Atherosclerosis 1999;144:15–23.

[21] van de Poll SW, Delsing DJ, Jukema JW, et al. Raman spectroscopic investigation of atorvastatin, amlodipine, and both on atherosclerotic plaque development in APOE*3 Leiden transgenic mice. Atherosclerosis 2002;164:65–71.

[22] Candido R, Allen TJ, Lassila M, et al. Irbesartan but not amlodipine suppresses diabetes-associated atherosclerosis. Circulation 2004;109:1536–42.

[23] Takai S, Kim S, Sakonjo H, Miyazaki M. Mechanisms of angiotensin II type 1 receptor blocker for anti-atherosclerotic effect in monkeys fed a high-cholesterol diet. J Hypertens 2003;21:361–9.

[24] Ma J, Kishida S, Wang GQ, et al. Comparative effects of azelnidipine and other Ca2+-channel blockers on the induction of inducible nitric oxide synthase in vascular smooth muscle cells. J Cardiovasc Pharmacol 2006;47:314–21.

[25] Shinomiya K, Mizushige K, Fukunaga M, et al. Antioxidant effect of a new calcium antagonist, azelnidipine, in cultured human arterial endothelial cells. J Int Med Res 2004;32:170–5.

[26] Lichtlen PR, Hugenholtz PG, Rafflenbeul W, et al. Retardation of angiographic progression of coronary artery disease by nifedipine. Results of the International Nifedipine Trial on Antiatherosclerotic Therapy (INTACT). INTACT Group investigators. Lancet 1990;335:1109–13.

[27] Jukema JW, Zwinderman AH, van Boven AJ, et al. Evidence for a synergistic effect of calcium channel blockers with lipid-lowering therapy in retarding progression of coronary atherosclerosis in symptomatic patients with normal to moderately raised cholesterol levels. The REGRESS Study Group. Arterioscler Thromb Vasc Biol 1996;16:425–30.

REGULAR PAPER

J. Physiol. Sci. Vol. 58, No. 3; Jun. 2008; pp. 189–198
Online May 13, 2008; **doi:10.2170/physiolsci.RP004308**

Upright Tilt Resets Dynamic Transfer Function of Baroreflex Neural Arc to Minify the Pressure Disturbance in Total Baroreflex Control

Atsunori KAMIYA[1], Toru KAWADA[1], Kenta YAMAMOTO[2], Masaki MIZUNO[1], Shuji SHIMIZU[1], and Masaru SUGIMACHI[1]

[1]Department of Cardiovascular Dynamics, National Cardiovascular Centre Research Institute, Osaka, Japan; and [2]Consolidated Research Institute for Advanced Science and Medical Care, Waseda University, Tokyo ,162-0041 Japan

Abstract: Maintenance of arterial pressure (AP) under orthostatic stress against gravitational fluid shift and pressure disturbance is of great importance. One of the mechanisms is that upright tilt resets steady-state baroreflex control to a higher sympathetic nerve activity (SNA). However, the dynamic feedback characteristics of the baroreflex system, a hallmark of fast-acting neural control, remain to be elucidated. In the present study, we tested the hypothesis that upright tilt resets the dynamic transfer function of the baroreflex neural arc to minify the pressure disturbance in total baroreflex control. Renal SNA and AP were recorded in ten anesthetized, vagotomized and aortic-denervated rabbits. Under baroreflex open-loop condition, isolated intracarotid sinus pressure (CSP) was changed according to a binary white noise sequence at operating pressure ± 20 mmHg, while the animal was placed supine and at 60° upright tilt. Regardless of the postures, the baroreflex neural (CSP to SNA) and peripheral (SNA to AP) arcs showed dynamic high-pass and low-pass characteristics, respectively. Upright tilt increased the transfer gain of the neural arc (resetting), decreased that of the peripheral arc, and consequently maintained the transfer characteristics of total baroreflex feedback system. A simulation study suggests that postural resetting of the neural arc would significantly increase the transfer gain of the total arc in upright position, and that in closed-loop baroreflex the resetting increases the stability of AP against pressure disturbance under orthostatic stress. In conclusion, upright tilt resets the dynamic transfer function of the baroreflex neural arc to minify the pressure disturbance in total baroreflex control.

Key words: baroreflex, blood pressure, sympathetic nervous system.

Since human beings are often under orthostatic stress, the maintenance of arterial pressure (AP) under orthostatic stress against gravitational fluid shift is of great importance. During standing, a gravitational fluid shift directed toward the lower part of the body would cause severe postural hypotension if not counteracted by compensatory mechanisms [1]. Arterial baroreflex has been considered to be the major compensatory mechanism [1–3], since denervation of baroreceptor afferents causes profound postural hypotension [4].

The baroreflex system consists of two subsystems: the neural arc that represents the input-output relationship between baroreceptor pressure and sympathetic nerve activity (SNA), and the peripheral arc that represents the relationship between SNA and systemic AP. Recently, we investigated the steady-state functional structure of these systems under orthostatic stress [5], and reported that upright tilt shifted the baroreflex peripheral arc to a lower AP for a given SNA. However, upright tilt reset the baroreflex neural arc to a higher steady state SNA. The resetting compensated for the blunted responsiveness of the peripheral arc and contributed to prevent postural hypotension [5].

In addition to the steady state characteristics [6, 7], the dynamic characteristics are other hallmark of the baroreflex system. It is because the system is a fast-acting neural control that quickly negative-feedback controls and stabilises AP against pressure disturbance in contrast to the slow-acting hormonal and humoral systems [8]. Earlier studies reported that the dynamic characteristics in supine position have a high-pass (fast) neural arc that may compensate for the low-pass (slow) peripheral arc to achieve rapid and stable AP regulation [8]. The importance of the dynamic characteristics in AP control increases under orthostatic stress that can cause postural hypotension. However, little is known about the dynamic characteristics of the baroreflex system in upright posture.

Because the gravitational body fluid shift decreases the effective circulatory blood volume [1, 9], we speculated that upright tilt may attenuate the dynamic transfer function from SNA to AP in the baroreflex peripheral arc.

Received on Mar 18, 2008; accepted on May 9, 2008; released online on May 13, 2008; doi:10.2170/physiolsci.RP004308
Correspondence should be addressed to: Atsunori Kamiya, Department of Cardiovascular Dynamics, National Cardiovascular Centre Research Institute, Osaka, 565-8565 Japan. Tel: +81-6-6833-5012, Fax: +81-6-6835-5403, E-mail: kamiya@ri.ncvc.go.jp

Moreover, if the upright tilt resets the dynamic characteristics of the neural arc in addition to resetting the steady state SNA reported previously [5], it would compensate for a blunted pressor response of the baroreflex peripheral arc and contribute to maintain the stability and quickness of the total baroreflex system. Accordingly, we hypothesized that upright tilt resets dynamic transfer function of baroreflex neural arc to minify the pressure disturbance in total baroreflex control.

In the present study, we identified the transfer functions of two baroreflex subsystems (the neural and peripheral arcs) separately in 60° upright posture, while opening the baroreflex negative feedback loop by vascular isolation of carotid sinus regions [8]. In addition, by connecting the subsystem transfer functions in series and closing them, we investigated the dynamic transfer characteristics and the stability against pressure disturbance of total baroreflex arc system in upright posture.

MATERIAL AND METHODS

Animals were cared for in strict accordance with the Guiding Principles for the Care and Use of Animals in the Field of Physiological Science approved by the Physiological Society of Japan. Ten Japanese white rabbits weighing 2.4–3.3 kg were initially anesthetized by intravenous injection (2 ml/kg) of a mixture of urethane (250 mg/ml) and α-chloralose (40 mg/ml). Anesthesia was maintained by continuously infusing the anaesthetics at a rate of 0.33 ml/kg/h using a syringe pump (CFV-3200, Nihon Kohden, Tokyo). The rabbits were mechanically ventilated with oxygen-enriched room air. Bilateral carotid sinuses were isolated vascularly from systemic circulation by ligating the internal and external carotid arteries and other small branches originating from the carotid sinus regions. The isolated carotid sinuses were filled with warmed physiological saline pre-equilibrated with atmospheric air, through catheters inserted via the common carotid arteries. Intra-carotid sinus pressure (CSP) was controlled by a servo-controlled piston pump (model ET-126A, Labworks; Costa Mesa, CA). Bilateral vagal and aortic depressor nerves were sectioned in the middle of the neck region to eliminate reflexes from the cardiopulmonary region and the aortic arch. Systemic AP was measured using a high-fidelity pressure transducer (Millar Instruments; Houston, TX) inserted retrograde from the right common carotid artery below the isolated carotid sinus region. Body temperature was maintained at around 38°C with a heating pad.

The left renal sympathetic nerve was exposed retroperitoneally. A pair of stainless steel wire electrodes (Bioflex wire AS633, Cooner Wire) was attached to the nerve to record renal SNA. The nerve fibers peripheral to electrodes were ligated securely and crushed to eliminate afferent signals. The nerve and electrodes were covered with a mixture of silicone gel (Silicon Low Viscosity, KWIK-SIL, World Precision Instrument, Inc., FL) to insulate and immobilize the electrodes. The preamplified SNA signal was band-pass filtered at 150–1,000 Hz. The nerve signal was full-wave rectified and low-pass filtered with a cutoff frequency of 30 Hz to quantify the nerve activity.

Protocols. Both protocols 1 and 2 were performed on each of eight animals. After the surgical preparation, the animal was maintained supine (0°) on a tilt bed. To stabilize the posture, the head was fixed full-frontal to the bed by strings, and the body and legs were rigged up in a clothes-like bag. Before performing protocols 1 and 2, we confirmed that the nerve activity measured in supine position was SNA. CSP was decreased stepwise from 100 mmHg to 40 mmHg in decrements of 20 mmHg, and then increased stepwise to 100 mmHg in increments of 20 mmHg. Each pressure step was maintained for 60 s. In all animals, a decrease in CSP increased SNA, whereas an increase in CSP decreased SNA (Fig. 1), indicating that the nerve activity recorded was SNA.

Protocol 1: The animal was placed supine. CSP was firstly matched with systemic AP to obtain the operating AP under the baroreflex closed-loop condition. After at least 5 minutes of stabilization, the SNA and AP were recorded for 10 min to obtain closed-loop baseline values. The data were stored on the hard disk of a dedicated laboratory computer system for analysis at a sampling rate of 200 Hz using a 12-bit analog-to-digital converter. The averaged AP over 10 min was defined as the operating AP in

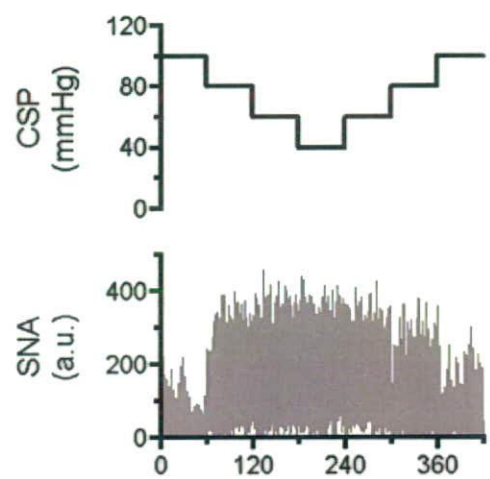

Fig. 1. Representative data of one rabbit in supine position, showing time series of carotid sinus pressure (CSP) and sympathetic nerve activity (SNA). CSP was decreased stepwise from 100 mmHg to 40 mmHg in decrements of 20 mmHg, and then increased stepwise to 100 mmHg in increments of 20 mmHg. Each pressure step was maintained for 60 s. A decrease in CSP increased SNA, whereas an increase in CSP decreased SNA, indicating that the nerve activity recorded was SNA. a.u., arbitrary unit.

supine position. Then, after at least 5 min of stabilization, CSP was randomly changed by 20 mmHg above or below the operating AP every 500 ms according to a binary white noise sequence for which the input power spectrum of CSP was reasonably flat up to 1 Hz [10]. The variables were recorded for a 10-min period and stored.

Protocol 2: CSP was firstly matched with systemic AP via a servo-controlled piston pump to obtain the actual operating pressure under baroreflex closed-loop conditions in supine and 60° upright postures. The animal was maintained supine for 10 min, and then tilted upright to 60° within 10 s by inclining the tilt bed to 60° and dropping the lower regions of the rabbit with the fulcrum set at the level of the carotid sinus. The 60° upright posture was maintained for 10 min for stabilization. Since the clothes-like bag stabilized the posture of the animal, there was no additional mechanical movement that reduced the quality of measurements. The position of the head remained almost fixed during the tilt to minimize vestibular stimulation. Thereafter, the average AP over the next 10 min was defined as the operating AP in upright tilt position. Then, after at least 5 min of stabilization, CSP was randomly changed according to a white noise sequence for 10 min as in protocol 1.

Data analysis. SNA signals were normalized by the following steps. First, the post-mortem noise level was assigned 0 arbitrary unit (a.u.). Second, SNA signals during the 10-min closed-loop baseline recording in protocol 1 (supine position) were averaged over 1 min, and assigned 100 a.u. Finally, the other SNA signals in all protocols were normalized to these values.

In both protocols 1 and 2, the transfer functions (gain and phase) and coherence function were calculated from CSP input to SNA in the baroreflex neural arc and from SNA input to AP in the baroreflex peripheral arc. The signals of CSP, SNA and AP were resampled at 10 Hz and segmented into 10 sets of 50% overlapping bins of 2^{10} data point each. The segment length was 102.4 s, which yielded the lowest frequency bound of 0.01 (0.0097) Hz. We subtracted a linear trend and applied a Hanning window for each segment. We then performed fast Fourier transform to obtain frequency spectra of the variables. We ensemble averaged the input power [$Sxx(f)$], output power [$Syy(f)$], and cross power between them [$Syx(f)$] over the 10 segments. Thereafter, we calculated the transfer function [$H(f)$] from input to output signals as follows,

$$H(f) = \frac{Syx(f)}{Sxx(f)}$$

To quantify the linear dependence between input to output signals in the frequency domain, we calculated the magnitude-squared coherence function [$Coh(f)$] as follows:

$$Coh(f) = \frac{|Syx(f)|^2}{Sxx(f)Syy(f)}$$

The coherence value ranges from zero to unity. Unity coherence indicates a perfect linear dependence between input and output signals, whereas zero coherence indicates total independence of these two signals.

Statistic analysis. All data are presented as means ± SD. Effects of upright tilt on baroreflex parameters were evaluated by repeated-measures analysis of variance. When the main effect was found to be significant, post hoc multiple comparisons were done using the Scheff's F-test to compare baroreflex controls between the supine and upright postures [11]. Differences were considered significant when $P < 0.05$.

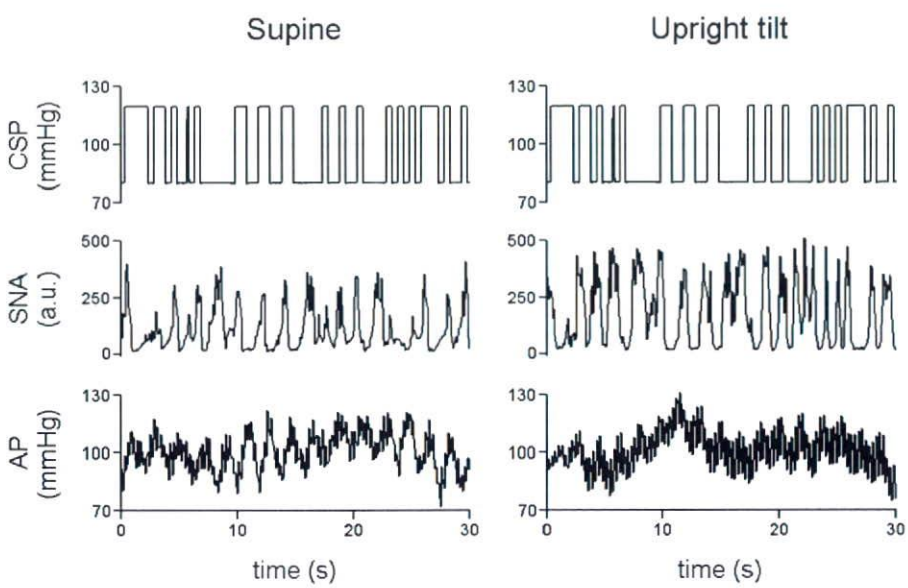

Fig. 2. Representative data of one rabbit in supine (left panels) and 60° upright tilt (right panels) positions, showing time series of carotid sinus pressure (CSP), sympathetic nerve activity (SNA) and systemic arterial pressure (AP) during CSP perturbation. CSP was changed according to a binary white noise signal with a switching interval of 500 ms. a.u., arbitrary unit.

RESULTS

Figure 2 shows the typical time series of CSP, SNA and AP derived in supine and 60° upright tilt positions in individual animal. CSP was perturbed according to a binary white noise sequence at 500-ms intervals. In both positions, SNA increased and decreased roughly in response to the decrease and increase in CSP, respectively. However, the SNA responses appeared higher in the upright tilt than in the supine position. Data from all animals (n = 8) showed that the upright tilt increased the averaged SNA (175 ± 21 a.u.) during CSP perturbation compared with the supine position (96 ± 13 a.u.). Averaged AP during CSP perturbation was similar in supine (96 ± 13 mmHg) and in upright positions (103 ± 15 mmHg).

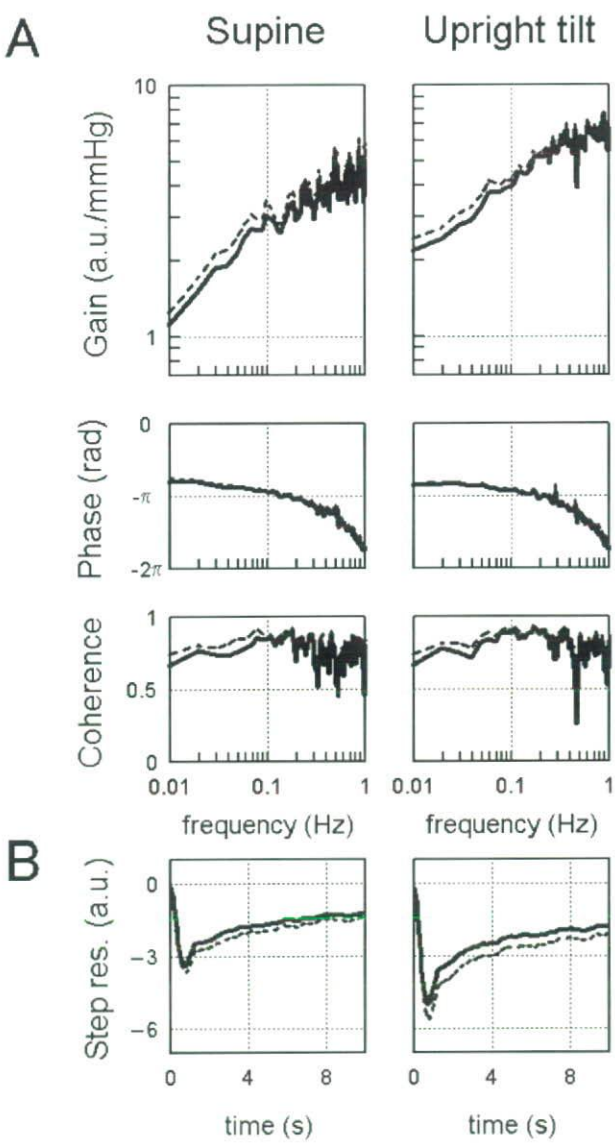

Fig. 3. A: The transfer function of the baroreflex neural arc from CSP to SNA averaged from all animals (n = 8) in supine (left panels) and 60° upright tilt (right panels) positions. The gain plots (top), phase plots (middle), and coherence function (bottom) are shown. Upright tilt increases the gain. **B**: Step responses (Step res.) derived from the transfer function corresponding to the transfer function shown in A. Upright tilt enhances the initial and steady-state responses. Solid line represents the mean values, and dashed line represents mean + SD in A and mean – SD in B. a.u., arbitrary unit.

The baroreflex neural arc

Figure 3A shows the transfer function of baroreflex neural arc from CSP to SNA averaged from all animals. In both supine and upright tilt positions, the transfer gain increased as the frequency of CSP perturbation increased for the frequency range of 0.01 to 1 Hz. This shows dynamic high-pass characteristics, indicating that more rapid change of CSP results in greater response of SNA. Note that upright tilt increased the transfer gain for the whole frequency range observed (Table 1). In addition, upright tilt decreased the slope of gain increase. In both positions, the phase approached slightly above $-\pi$ radians at the lowest frequency reflecting negative feedback characters, and lagged as the frequency of CSP perturbation increased. The coherence was over 0.7 for the frequency range of 0.01 to 0.2 Hz. Upright tilt did not affect the phase or coherence. Figure 3B shows the step response of SNA corresponding to the transfer function shown in Fig. 3A. In both positions, the SNA response consisted of an initial decrease followed by partial recovery and then a steady state. Of note, upright tilt enhanced the initial decrease by 50%, and also decreased the steady-state SNA.

Table 1. Transfer function of baroreflex neural arc (from CSP to SNA) in supine and upright tilt positions.

	Supine	Upright tilt
Gain (a.u./mmHg)		
0.01 Hz	1.11 ± 0.13	2.14 ± 0.41*
0.1 Hz	2.75 ± 0.43	4.63 ± 0.52*
0.3 Hz	3.69 ± 0.30	5.08 ± 0.42*
Phase (rad)		
0.01 Hz	−2.51 ± 0.15	−2.66 ± 0.09
0.1 Hz	−2.96 ± 0.08	−2.93 ± 0.06
0.3 Hz	−3.58 ± 0.14	−3.53 ± 0.12
Coherence		
0.01 Hz	0.67 ± 0.08	0.67 ± 0.07
0.1 Hz	0.84 ± 0.04	0.89 ± 0.02
0.3 Hz	0.77 ± 0.06	0.82 ± 0.03
Slope (dB/decade)		
0.01 Hz to 0.3 Hz	7.0 ± 0.4	5.1 ± 0.5*
Step response (a.u.)		
Initial response	−3.41 ± 0.21	−4.99 ± 0.62*
Steady-state level	−1.26 ± 0.18	−1.80 ± 0.32*

Values are mean ± SD (n =10). *P < 0.05; supine position vs. upright tilt.

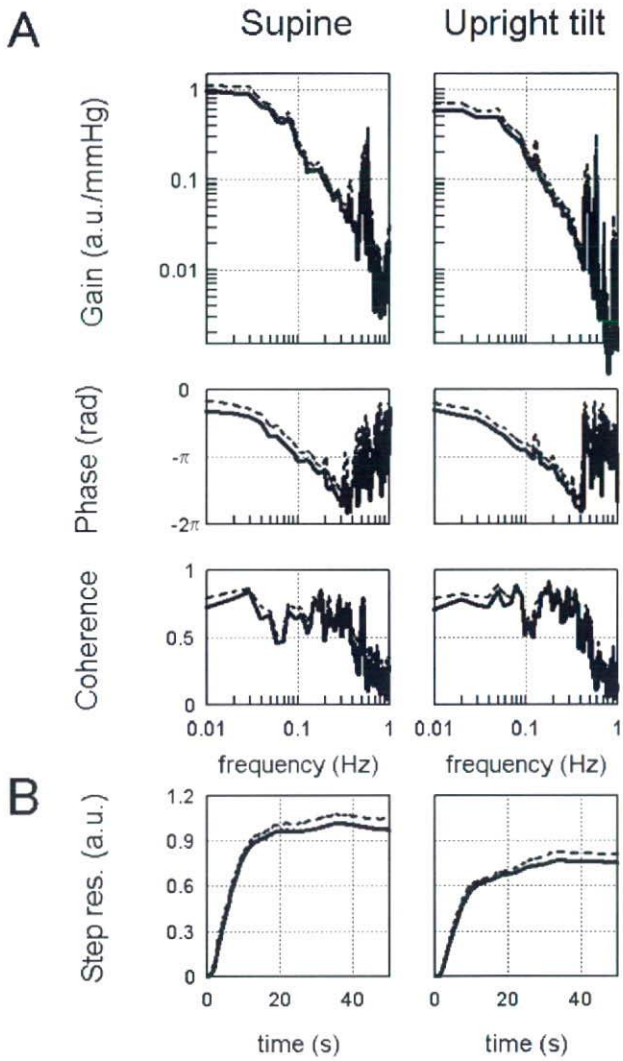

Fig. 4. A: The transfer function of the baroreflex peripheral arc from SNA to AP averaged from all animals (n = 8) in supine (left panels) and 60° upright tilt (right panels) positions. The gain plots (top), phase plots (middle), and coherence function (bottom) are shown. Upright tilt decreases the gain below the frequency of 0.1 Hz. **B**: Step responses (Step res.) derived from the transfer function corresponding to the transfer function shown in A. Upright tilt attenuates the response. Solid and dashed lines represent the mean and mean + SD values, respectively. a.u., arbitrary unit.

Table 2. Transfer function of baroreflex peripheral arc (from SNA to AP) in supine and upright tilt positions.

	Supine	Upright tilt
Gain (mmHg/au)		
0.01 Hz	0.97 ± 0.09	0.63 ± 0.06*
0.1 Hz	0.23 ± 0.03	0.15 ± 0.03*
0.3 Hz	0.04 ± 0.006	0.03 ± 0.003
Phase (rad)		
0.01 Hz	−0.79 ± 0.16	−0.69 ± 0.07
0.1 Hz	−2.83 ± 0.14	−2.58 ± 0.15
0.3 Hz	−4.74 ± 0.18	−4.63 ± 0.08
Coherence		
0.01 Hz	0.72 ± 0.07	0.71 ± 0.03
0.1 Hz	0.64 ± 0.08	0.62 ± 0.04
0.3 Hz	0.61 ± 0.08	0.68 ± 0.02
Step response (mmHg)		
Steady-state level	−0.97 ± 0.06	−0.75 ± 0.06*

Values are mean ± SD (n =10). *P < 0.05; supine position vs. upright tilt.

The baroreflex peripheral arc

Figure 4A shows the transfer function of the baroreflex peripheral arc from SNA to AP averaged from all animals. In both supine and upright tilt positions, the transfer gain decreased as the input frequency increased for the frequency range of 0.01 to 1 Hz, indicating low-pass characteristics. Upright tilt decreased the transfer gain between 0.01 and 0.1 Hz (Table 2). In both positions, the phase approached zero radian at the lowest frequency reflecting an increase in SNA with increased AP, and lagged as the input frequency increased. The coherence was over 0.5 for the frequency range of 0.01 to 1 Hz. Upright tilt did not affect the phase or coherence. Figure 4B shows the step response of AP corresponding to the transfer function shown in Fig. 4A. In both positions, the AP response increased gradually to reach a steady state. Upright tilt decreased the steady-state AP.

The total baroreflex arc

Figure 5A shows the transfer function of the total baroreflex arc from CSP to AP averaged from all animals. In both supine and upright tilt positions, the transfer gain decreased as the input frequency increased for the frequency range from 0.01 to 1 Hz, indicating low-pass characteristics. Upright tilt did not affect the transfer gain (Table 3). In both positions, the phase approached $-\pi$ radians at the lowest frequency reflecting negative feedback attained by the total baroreflex loop, and lagged as the input frequency increased. The coherence was over 0.5 for the frequency range from 0.01 to 0.2 Hz. Upright tilt did not affect the phase or coherence. Figure 5B shows the step response of AP corresponding to the transfer function shown in Fig. 5A. In both positions, the AP response increased gradually to reach a steady state. Upright tilt did not affect the step response.

The right column of Table 3 shows a simulation of the total arc transfer function in the absence of resetting in the neural arc. The simulation was based on the neural arc transfer function in supine position and the peripheral arc transfer function in upright tilt position. Without the resetting, the upright tilt would decrease the transfer function gain and would attenuate the step response of AP at steady state, compared with the values in supine position and those in upright tilt position with resetting.

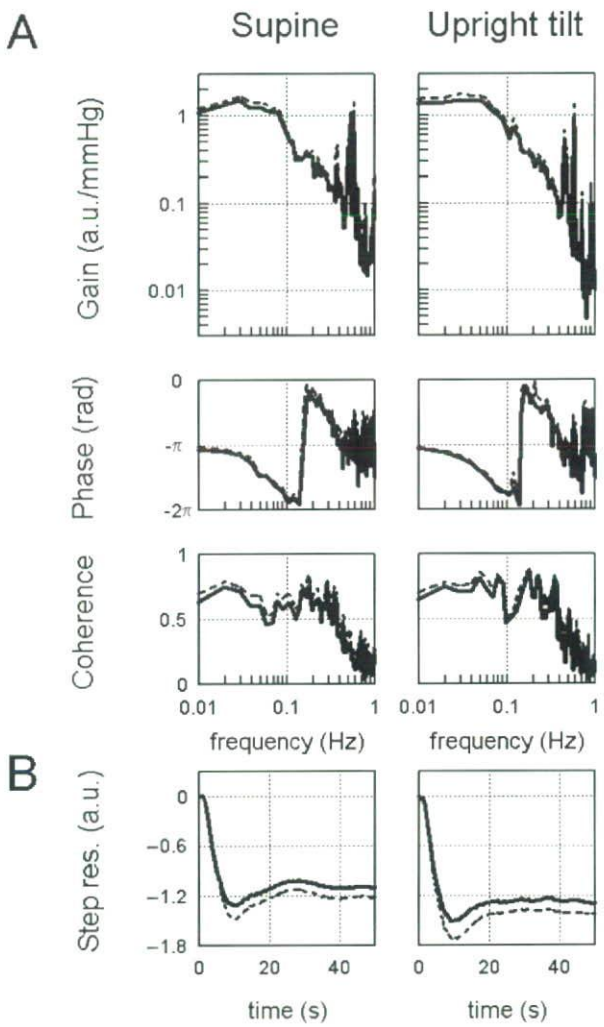

Fig. 5. A: The transfer function of the total baroreflex arc from CSP to AP averaged from all animals (n = 8) in supine (left panels) and 60° upright tilt (right panels) positions. The gain plots (top), phase plots (middle), and coherence function (bottom) are shown. **B**: Step responses (Step res.) derived from the transfer function corresponding to the transfer function shown in A. The transfer function and step response are similar in the supine and upright tilt positions. Solid and dashed lines represent the mean and mean + SD values in A and mean – SD values in B, respectively. a.u., arbitrary unit.

DISCUSSION

Arterial baroreflex is obviously a pivotal mechanism for maintaining AP under orthostatic stress against gravitational fluid shift and pressure disturbance [1, 2, 4], but the baroreflex function and its modulation in upright position are not fully understood. We previously reported that 60° upright tilt resets the steady-state characteristics of the baroreflex neural arc to a higher SNA [5]. However, the dynamic characteristics of the baroreflex system, which is a hallmark of fast-acting neural systems, in upright posture remain to be elucidated. Accordingly, in the present study, we identified the transfer function of the total baroreflex system and its two subsystems. The new major findings are that a 60° upright tilt increases the transfer gain of the baroreflex neural arc (CSP to SNA), decreases the transfer gain of the peripheral arc (SNA to AP), and as a result maintains the dynamic characteristics of the total baroreflex feedback system. These findings support our hypothesis that upright tilt resets dynamic transfer function of baroreflex neural arc to minify the pressure disturbance in total baroreflex control. These results were not affected by the order of postures, since returning the ani-

Table 3. Transfer function of total baroreflex arc (from CSP to AP) in supine, upright tilt and simulated upright tilt positions.

	Supine	Upright tilt	Simulated upright tilt without resetting of the neural arc
Gain (a.u./mmHg)			
0.01 Hz	1.10 ± 0.12	1.38 ± 0.18	0.71 ± 0.18*#
0.1 Hz	0.63 ± 0.09	0.69 ± 0.12	0.41 ± 0.13*#
0.3 Hz	0.15 ± 0.03	0.15 ± 0.03	0.11 ± 0.04*
Phase (rad)			
0.01 Hz	−3.33 ± 0.11	−3.29 ± 0.07	−3.21 ± 0.10
0.1 Hz	−5.76 ± 0.20	−5.55 ± 0.10	−5.51 ± 0.15
0.3 Hz	−1.98 ± 0.25	−1.87 ± 0.23	−1.91 ± 0.24
Coherence			
0.01 Hz	0.63 ± 0.06	0.65 ± 0.05	
0.1 Hz	0.60 ± 0.10	0.61 ± 0.06	
0.3 Hz	0.53 ± 0.07	0.55 ± 0.04	
Step response (mmHg)			
Steady-state level	−1.09 ± 0.11	−1.29 ± 0.12	−0.67 ± 0.11*#

Simulated transfer function in the absence of neural arc resetting is calculated from the neural arc transfer function in supine position and the peripheral arc transfer function in upright tilt position. Values are mean ± SD (n =10). *P < 0.05; supine vs. simulated upright tilt, #P < 0.05; upright tilt vs. simulated upright tilt.

mal posture from 60° upright tilt to horizontal supine position restored the transfer functions to the magnitudes observed in the initial supine position (data not shown).

Little is known about the arterial baroreflex feedback system under orthostatic stress. Although earlier studies investigated the gains of baroreflex control of SNA [12–14], vascular resistance [15] and R-R interval [16], these gains are parts of the total baroreflex system, and thus are insufficient to explain the dynamics of the total arc of the baroreflex feedback system. In addition, no study has examined the phase function of baroreflex in the subsystems and the total system. Moreover, while earlier studies addressed baroreflex in relation to AP regulation under orthostatic stress, most of them evaluated the baroreflex in supine, and not orthostatic posture [14]. In the present study, we identified the transfer functions of the two baroreflex subsystems (the neural and peripheral arcs) in upright posture independently using the baroreflex open-loop technique. Moreover, by connecting the subsystem transfer functions in series and closing them, we revealed the dynamic characteristics of the total baroreflex arc.

Our actual and simulation data indicated that resetting of the baroreflex neural arc in upright posture increases the transfer function gain of the total baroreflex arc. In our experiments, the 60° upright tilt reset and nearly doubled the transfer gain of the neural arc. Although the upright tilt decreased the transfer gain of the peripheral arc, resetting in the neural arc counteracted it and consequently preserved the dynamic transfer gain of the total baroreflex arc (1.4, Table 3). In a simulation of a situation where resetting in the neural arc is absent (Table 3), a 60° upright tilt would decrease the total arc transfer gain. These findings suggest that resetting of the neural arc (that is, baroreflex control of SNA) with dynamic characteristics plays an im-

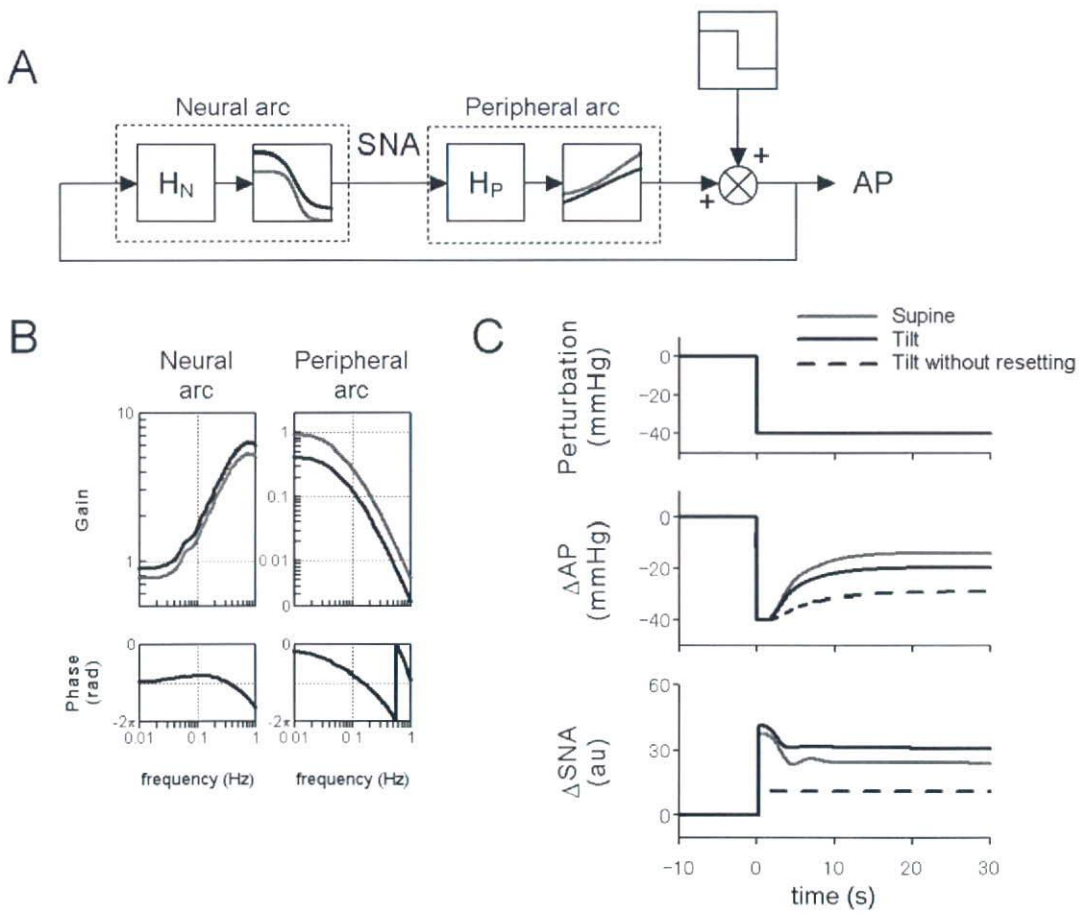

Fig. 6. A: Simulator of the baroreflex system during upright tilt. A stepwise perturbation was applied to the baroreflex negative feedback system (see APPENDIX for details). H_N, neural arc transfer function; H_P, peripheral arc transfer function. Nonlinear sigmoidal functions in the supine and upright tilt positions are shown by gray and black lines, respectively. **B**: Simulation results of integrated dynamic transfer function of linear-sigmoidal nonlinear cascade model in the neural (AP to SNA) and peripheral (SNA to AP) arcs in the supine (gray lines) and upright tilt (black lines) positions. **C**: Simulation results of a closed-loop AP and SNA responses to the stepwise pressure perturbation (–40 mmHg). The resetting during upright tilt (black line) would enhance SNA excitation as compared with the supine position (gray line) to minify a hypotension. Without the resetting in upright tilt, SNA responses would largely be attenuated to lead a hypotension.

portant role to maintain the dynamic transfer function of the total baroreflex system in upright posture.

A simulation of AP stability by baroreflex feedback control against pressure disturbance clearly suggests the importance of resetting of baroreflex neural arc in upright posture. Figure 6 shows the simulation of closed-loop baroreflex control of AP, when pressure disturbance was loaded to the peripheral cardiovascular compartment. According to an earlier study [17], we used the linear-sigmoidal nonlinear cascade model (Fig. 6A) to simulate the baroreflex dynamics. The result of simulation (Fig. 6B) was consistent with our in vivo findings that an upright tilt increased the dynamic transfer gain of the neural arc and decreased the dynamic gain of the peripheral arc. The simulation (Fig. 6C) shows that the baroreflex feedback system would minify the pressure disturbance (40 mmHg) by 50% or more in supine (14 mmHg) and upright tilt (19 mmHg) positions. However, without the resetting of the neural arc in upright tilt, the residual pressure disturbance (29 mmHg) would persist and the velocity of pressure response would become slower (Fig. 6C). These findings suggest that dynamic resetting of the neural arc increases the stability and quickness in response of orthostatic AP against pressure disturbance in closed-loop condition of the total baroreflex arc. In addition, the simulation indicates that the resetting would enhance increases in SNA in response to pressure disturbance in upright tilt compared to supine position (Fig. 6C). Without the resetting in upright tilt, the SNA response would be greatly attenuated (Fig. 6C). This suggests that resetting of the neural arc has a critical role in activating SNA appropriately to prevent hypotension by pressure disturbance during orthostatic stress.

Some explanations for the changes in baroreflex peripheral arc in upright tilt posture may be postulated. First, since the gravitational fluid shift toward the lower part of body (i.e., abdominal vascular bed, lower limbs) during upright posture decreases the preload and effective circulatory blood volume [1, 9], it may attenuate the dynamic transfer function from SNA to AP. Our actual data revealed that upright tilt decreased the transfer gain, but not the transfer phase, of the baroreflex peripheral arc (Fig. 4A). Therefore, upright tilt would blunt the magnitude of AP response to SNA without delaying the response, as shown in the calculated step response (Fig. 4B). Next, increases in humoral factors (i.e., catecholamine, angiotensin II) during upright posture could reduce the dependency of vascular resistance on neural control. However, intravenous infusion of angiotensin II did not affect the transfer function of baroreflex peripheral arc [18]. Moreover, intravenous infusion of catecholamine had no effects on the transfer function from sympathetic stimulation to heart rate [19]. These studies are consistent with the predominance of sympathetic neural control on cardiovascular pressor function [20].

Limitations

The present study has several limitations. First, we excluded the efferent effect of vagally mediated arterial and cardiopulmonary baroreflexes that may affect baroreflex control of SNA. Second, we used an anesthetic agent that may attenuate the baroreflex peripheral arc by reducing the cardiac pumping function, and may affect the neural arc gain. Third, since we sectioned the aortic depressor nerves to open the baroreflex feedback loop, the total baroreflex gain may be lower than the physiological level. Fourth, since we measured only renal SNA, our findings have limited applicability to other SNA. Although static [10, 21] and dynamic [21] regulation of the baroreflex neural arc is similar in renal, cardiac and muscle (vasoconstrictor) SNAs in supine posture, whether this holds true during orthostatic stress remains to be verified.

Lastly, we used rabbits that are quadrupeds. Since humans spend most of their time in nearly 90° upright postures whereas rabbits do not, our findings have limited applicability to humans. However, Japanese White rabbits spend most of their time in 10–40° head-up postures, and frequently stand up to nearly 70°. Since the denervation of both carotid and aortic arterial baroreflexes is known to cause severe postural hypotension at 60° upright tilt in quadrupeds [4], this suggests that even in quadrupeds, arterial baroreflex has a very important function in the maintenance of AP under orthostatic stress. Accordingly, despite the difference in species, our findings may reflect, at least, the qualitative aspects of orthostatic baroreflex physiology in humans. Indeed, recent human studies have suggested that orthostatic stress (lower body negative pressure) enhances the SNA response to AP change [22, 23] and increases baroreflex control of SNA (assessed by the relation between spontaneous changes in diastolic AP and SNA) [12] under baroreflex closed-loop condition.

In conclusion, the transfer function identified in baroreflex open-loop condition showed that 60° upright tilt increases the transfer gain of the baroreflex neural arc, decreases the transfer gain of the peripheral arc, and as a result maintains the dynamic characteristics of the total baroreflex feedback system. Simulation study suggests that resetting of the neural arc increases the transfer gain of the total baroreflex arc and also increases the stability of orthostatic AP against pressure disturbance. These findings suggest that upright tilt resets the dynamic transfer function of the baroreflex neural arc to maintain total baroreflex stability.

APPENDIX

To simulate the closed-loop AP response to stepwise pressure perturbation (Fig. 6), we used the linear-sigmoidal nonlinear cascade model [17].

We modeled the sigmoidal nonlinearity in the baroreflex neural arc by a four-parameter logistic function with

threshold according to our previous study [5] using the following equation:

$$y = \frac{P_1}{1+\exp[P_2(x-P_3)]} + P_4$$

where x and y are input (in mmHg) and output (in au) values. P_1 denotes the response range (in a.u.), P_2 is the coefficient of gain, P_3 is the midpoint of the input range (in mmHg), P_4 is the minimum output value of the symmetric sigmoid curve (in a.u.). We set $P_1 = 94$, $P_2 = 0.10$, $P_3 = 109$, $P_4 = 4$ in the supine position, and $P_1 = 112$, $P_2 = 0.09$, $P_3 = 109$, $P_4 = 29$ during upright tilt, according to our previous study [5].

The sigmoidal nonlinearity in the peripheral arc was modeled by a four-parameter logistic function using the following equation:

$$z = \frac{Q_1}{1+\exp[Q_2(y-Q_3)]} + Q_4$$

where y and z are input (in a.u.) and output (in mmHg) values. Q_1 denotes the response range (in mmHg), Q_2 is the coefficient of gain, Q_3 is the midpoint of the input range (in a.u.), and Q_4 is the minimum output value (in mmHg). We set $Q_1 = 115$, $Q_2 = -0.04$, $Q_3 = 63$, $Q_4 = 50$ in the supine position, and $Q_1 = 82$, $Q_2 = -0.05$, $Q_3 = 88$, $Q_4 = 50$ during upright tilt, according to our previous study [5].

In rabbits, the transfer function of the baroreflex neural arc (baroreceptor pressure to SNA) approximates derivative characteristics in the frequency range below 0.8 Hz, and high-cut characteristics of frequencies above 0.8 Hz [17]. Therefore, according to our previous study [17], we modeled the neural arc transfer function (H_N) using the following equation:

$$H_N(f) = -K_N \frac{1+\frac{f}{f_{c1}}j}{\left(1+\frac{f}{f_{c2}}\right)^2}\exp(-2\pi fjL)$$

where f and j represent the frequency (in Hz) and imaginary units, respectively; K_N is static gain (in a.u./mmHg); f_{c1} and f_{c2} ($fc_1 < f_{c2}$) are corner frequencies (in Hz) for derivative and high-cut characteristics, respectively; and L is a pure delay (in s) that would represent the sum of delays in the synaptic transmission through the baroreflex central pathways and the sympathetic ganglion. The dynamic gain increases in the frequency range of f_{c1} to f_{c2}, and decreases above f_{c2}. In simulations showed in Fig. 6, we matched K_N to the actual data in the supine and upright tilt positions in this study. We also set f_{c1}, f_{c2} and L at 0.05, 0.8 and 0.2, respectively, according to the present and previous studies [17].

In addition, the transfer function of the baroreflex peripheral arc (SNA to AP) approximates a second-order low-pass filter with the dead time as follows:

$$H_P(f) = K_P \frac{1}{1+2\zeta\frac{f}{f_N}j-\left(\frac{f}{f_N}\right)^2}\exp(-2\pi fjL)$$

where f_N and ζ are the neutral frequency (in Hz) and damping ratio, respectively; and L is a pure delay (in s). In simulations showed in Fig. 6, we matched K_P to the actual data in the supine and upright tilt positions in this study. We also set f_N, ζ and L at 0.07, 1.4 and 1.0, respectively, according to the present and previous studies [17].

The input amplitude of the stepwise pressure perturbation was –40 mmHg (Fig. 5, A and C, top panel). The closed-loop AP (Fig. 5C, middle panel) and SNA (Fig. 5C, bottom panel) responses were simulated up to 30 s.

This study was supported by the research project promoted by Ministry of Health, Labour and Welfare in Japan (#H18-nano-ippan-003), the Grants-in-Aid for Scientific Research promoted by Ministry of Education, Culture, Sports, Science and Technology in Japan (#18591992, #20390462) and the Industrial Technology Research Grant Program from New Energy and Industrial Technology Development Organization of Japan.

REFERENCES

1. Rowell LB. Human cardiovascular control. New York: Oxford Univ. Press, 1993.
2. Eckberg DL, Sleight P. Human baroreflexes in Health and Disease. New York: Oxford Univ. Press, 1992.
3. Persson P, Kirchheim H. Baroreceptor reflexes: integrative functions and clinical aspects. Berlin: Springer-Verlag, 1991.
4. Sato T, Kawada T, Sugimachi M, Sunagawa K. Bionic technology revitalizes native baroreflex function in rats with baroreflex failure. Circulation. 2002;106:730-4.
5. Kamiya A, Kawada T, Yamamoto K, Michikami D, Ariumi H, Uemura K, et al. Resetting of the arterial baroreflex increases orthostatic sympathetic activation and prevents postural hypotension in rabbits. J Physiol. 2005;566:237-46.
6. Sato T, Kawada T, Inagaki M, Shishido T, Takaki H, Sugimachi M, et al. New analytic framework for understanding sympathetic baroreflex control of arterial pressure. Am J Physiol. 1999;276:H2251-61.
7. Yamamoto K, Kawada T, Kamiya A, Takaki H, Miyamoto T, Sugimachi M, et al. Muscle mechanoreflex induces the pressor response by resetting the arterial baroreflex neural arc. Am J Physiol. 2004;286:H1382-8.
8. Ikeda Y, Kawada T, Sugimachi M, Kawaguchi O, Shishido T, Sato T, et al. Neural arc of baroreflex optimizes dynamic pressure regulation in achieving both stability and quickness. Am J Physiol. 1996;271:H882-90.
9. Sagawa K, Maughan L, Suga H, Sunagawa K. Cardiac contraction and the pressure-volume relationship. New York: Oxford Univ Press, 1988.
10. Kawada T, Shishido T, Inagaki M, Tatewaki T, Zheng C, Yanagiya Y, et al. Differential dynamic baroreflex regulation of cardiac and renal sympathetic nerve activities. Am J Physiol Heart Circ Physiol. 2001;280:H1581-90.
11. Glantz SA. Primer of Biostatistics (4th ed). New York: McGraw-Hill, 1997.
12. Ichinose M, Saito M, Fujii N, Kondo N, Nishiyasu T. Modulation of the control of muscle sympathetic nerve activity during severe orthostatic stress. J Physiol. 2006;576:947-58.
13. Fu Q, Shook RP, Okazaki K, Hastings JL, Shibata S, Conner CL, et al. Vasomotor sympathetic neural control is maintained during sustained upright posture in humans. J Physiol (Lond). 2006;577:679-87.
14. Mosqueda-Garcia R, Furlan R, Fernandez-Violante R, Desai T, Snell M, Jarai Z, et al. Sympathetic and baroreceptor reflex function in neurally mediated syncope evoked by tilt. J Clin Invest. 1997;99:2736-44.
15. Cooper VL, Hainsworth R. Carotid baroreceptor reflexes in humans during orthostatic stress. Exp Physiol. 2001;86:677-81.
16. Cooke WH, Hoag JB, Crossman AA, Kuusela TA, Tahvanainen KU, Eckberg DL.

Human responses to upright tilt: a window on central autonomic integration. J Physiol. 1999;517:617-28.
17. Kawada T, Yanagiya Y, Uemura K, Miyamoto T, Zheng C, Li M, et al. Input-size dependence of the baroreflex neural arc transfer characteristics. Am J Physiol Heart Circ Physiol. 2003;284:H404-15.
18. Kashihara K, Takahashi Y, Chatani K, Kawada T, Zheng C, Li M, et al. Intravenous angiotensin II does not affect dynamic baroreflex characteristics of the neural or peripheral arc. Jpn J Physiol. 2003;53:135-43.
19. Kawada T, Miyamoto T, Miyoshi Y, Yamaguchi S, Tanabe Y, Kamiya A, et al. Sympathetic neural regulation of heart rate is robust against high plasma catecholamines. J Physiol Sci. 2006;56:235-45.
20. Minson J, Chalmers J, Kapoor V, Cain M, Caon A. Relative importance of sympathetic nerves and of circulating adrenaline and vasopressin in mediating hypertension after lesions of the caudal ventrolateral medulla in the rat. J Hypertens. 1986;4:273-81.
21. Kamiya A, Kawada T, Yamamoto K, Michikami D, Ariumi H, Miyamoto T, et al. Muscle sympathetic nerve activity averaged over 1 minute parallels renal and cardiac sympathetic nerve activity in response to a forced baroreceptor pressure change. Circulation. 2005;112:384-6.
22. Ichinose M, Saito M, Ogawa T, Hayashi K, Kondo N, Nishiyasu T. Modulation of control of muscle sympathetic nerve activity during orthostatic stress in humans. Am J Physiol Heart Circ Physiol. 2004;287:H2147-53.
23. Ichinose M, Saito M, Kitano A, Hayashi K, Kondo N, Nishiyasu T. Modulation of arterial baroreflex dynamic response during mild orthostatic stress in humans. J Physiol. 2004;557:321-30.

Life Sciences 83 (2008) 490–495

Contents lists available at ScienceDirect

Life Sciences

journal homepage: www.elsevier.com/locate/lifescie

Vagal stimulation suppresses ischemia-induced myocardial interstitial myoglobin release

Toru Kawada [a,*], Toji Yamazaki [b], Tsuyoshi Akiyama [b], Hirotoshi Kitagawa [c], Shuji Shimizu [a], Masaki Mizuno [a], Meihua Li [a], Masaru Sugimachi [a]

[a] Department of Cardiovascular Dynamics, Advanced Medical Engineering Center, National Cardiovascular Center Research Institute, Osaka 565-8565, Japan
[b] Department of Cardiac Physiology, National Cardiovascular Center Research Institute, Osaka 565-8565, Japan
[c] Department of Anesthesiology, Shiga University of Medical Science, Shiga 520-2192, Japan

ARTICLE INFO

Article history:
Received 19 May 2008
Accepted 23 July 2008

Keywords:
Coronary artery occlusion
Cardiac microdialysis
Cats

ABSTRACT

Aims: To evaluate vagal stimulation-mediated myocardial protection against ischemia and reperfusion in in vivo ischemic myocardium.
Main methods: We measured myocardial interstitial myoglobin levels in the ischemic region using a cardiac microdialysis technique in anesthetized and vagotomized cats. We occluded the left anterior descending coronary artery (LAD) for 60 min and reperfused it for 60 min (VX group, $n=6$). The effects of bilateral vagal stimulation (10 V, 5 Hz, 1-ms pulse duration), initiated immediately after LAD occlusion, were examined (VS group, $n=6$). To examine the involvement of phosphatidylinositol 3-kinase (PI3K), vagal stimulation was performed after pretreatment with a PI3K inhibitor wortmannin (0.6 mg/kg, i.v.) (VS-W group, $n=6$). To examine the contribution of bradycardia, vagal stimulation was performed with fixed-rate ventricular pacing (VS-P group, $n=6$).
Key findings: The average myoglobin level during the ischemic period was 1170±141 in VX (in ng/ml, mean±SE), which was significantly attenuated in VS (466±87, $P<0.05$) and VS-W (613±124, $P<0.05$) but not in VS-P (953±203). Reperfusion increased the myoglobin level to 2500±544 in VX, whereas it was suppressed in VS (824±213, $P<0.05$) and VS-W (948±315, $P<0.05$) but not in VS-P (1710±253).
Significance: Vagal stimulation, initiated immediately after LAD occlusion, attenuated the myocardial injury. Moreover, bradycardia, independent of PI3K pathway, plays a significant role in vagally induced cardioprotection during acute myocardial ischemia.

Introduction

An increase in parasympathetic tone can provide cardioprotection against acute myocardial ischemia and infarction via the direct effects of acetylcholine (ACh) on the ischemic myocardium and the indirect effects mediated by altered hemodynamics. For the direct effects, administration of ACh prior to a coronary artery occlusion reduces the infarct size in isolated, perfused rabbit heart (Qin et al., 2003). Phosphatidylinositol 3-kinase (PI3K) is thought to be an upstream enzyme in the signal transduction pathway for the ACh-induced, ischemic preconditioning mimetic effect (Qin et al., 2003; Oldenburg et al., 2003). For the indirect effects, vagal stimulation reduces myocardial oxygen consumption due to bradycardia (Sammel et al., 1983) and also decreases ventricular contractility via antagonism of the sympathetic effect (Nakayama et al., 2001). Vagal stimulation can also dilate the coronary artery (Feigl, 1969; Reid et al., 1985; Feliciano and Henning, 1998; Henning and Sawmiller, 2001), which may increase collateral flow into the ischemic region.

In a previous study, we demonstrated that efferent vagal stimulation nearly halved the increase in myocardial interstitial norepinephrine levels in the ischemic region of the feline ventricle (Kawada et al., 2006). Whether vagal stimulation can reduce myocardial damage in the ischemic region, however, has yet to be directly examined. To test the hypothesis that vagal stimulation reduces myocardial injury in the ischemic region, we measured myocardial interstitial myoglobin levels during acute myocardial ischemia and reperfusion with or without efferent vagal stimulation in anesthetized cats. We examined possible involvement of the PI3K signaling pathway using vagal stimulation and pretreatment with a PI3K inhibitor wortmannin. We also examined the contribution of bradycardia using vagal stimulation and fixed-rate ventricular pacing.

Materials and methods

Surgical preparation

Animal care was provided in strict accordance with the *Guiding Principles for the Care and Use of Animals in the Field of Physiological Sciences* approved by the Physiological Society of Japan. Adult cats

* Corresponding author. Department of Cardiovascular Dynamics, National Cardiovascular Center Research Institute, 5-7-1 Fujishirodai, Suita, Osaka 565-8565, Japan. Tel.: +81 6 6833 5012x2427; fax: +81 6 6835 5403.
E-mail address: torukawa@res.ncvc.go.jp (T. Kawada).

0024-3205/$ – see front matter © 2008 Elsevier Inc. All rights reserved.
doi:10.1016/j.lfs.2008.07.013